Published in final edited form as:
Nat Neurosci. 2016 April ; 19(4): 605–612. doi:10.1038/nn.4251.

4 Hz oscillations synchronize prefrontal-amygdala circuits during fear behaviour

Nikolaos Karalis[1,2,3,6,8], **Cyril Dejean**[1,2,6], **Fabrice Chaudun**[1,2,6], **Suzana Khoder**[1,2], **Robert R. Rozeske**[1,2], **Hélène Wurtz**[1,2], **Sophie Bagur**[4], **Karim Benchenane**[4], **Anton Sirota**[3], **Julien Courtin**[1,2,5,7], and **Cyril Herry**[1,2,7,8]

[1]INSERM, Neurocentre Magendie, U862, 146 Rue Léo-Saignat, 33077 Bordeaux, France. [2]Univ. Bordeaux, Neurocentre Magendie, U862, 146 Rue Léo-Saignat, 33077 Bordeaux, France. [3]Bernstein Center for Computational Neuroscience Munich, Munich Cluster of Systems Neurology (SyNergy), Faculty of Medicine, Ludwig-Maximilians Universität München, 82152 Planegg-Martinsried, Germany. [4]Team Memory, Oscillations and Brain states (MOBs), Brain Plasticity Unit, CNRS UMR 8249, ESPCI ParisTech. Ecole Supérieure de Physique et de Chimie Industrielles de la Ville de Paris, 10 rue Vauquelin, 75005 Paris, France. [5]Friedrich Miescher Institute for Biomedical Research, Maulbeerstrasse 66, CH-4058 Basel, Switzerland.

Abstract

Fear expression relies on the coordinated activity of prefrontal and amygdala circuits, yet the mechanisms allowing long-range network synchronization during fear remain unknown. Using a combination of extracellular recordings, pharmacological, and optogenetic manipulations we report that freezing, a behavioural expression of fear, temporally coincides with the development of sustained, internally generated 4 Hz oscillations within prefrontal-amygdala circuits. 4 Hz oscillations predict freezing onset and offset and synchronize prefrontal-amygdala circuits. Optogenetic induction of prefrontal 4 Hz oscillations coordinates prefrontal-amygdala activity and elicits fear behaviour. These results unravel a novel sustained oscillatory mechanism mediating prefrontal-amygdala coupling during fear behaviour.

Introduction

Long-range neuronal synchronization among groups of neurons is an effective mechanism that promotes the transmission of information between neuronal structures[1-4]. This form of neuronal communication has been largely described in sensory and motor systems[5-8] and

[8]To whom correspondence should be addressed. cyril.herry@inserm.fr (CH); karalis@bio.lmu.de (NK) .

Author Contributions

S. Bagur, K. Benchenane, F. Chaudun, J. Courtin, C. Dejean, N. Karalis, S. Khoder, R.R. Rozeske, A. Sirota, and H. Wurtz performed the experiments and analyzed the data. J. Courtin, C. Dejean, N. Karalis and C. Herry designed the experiments. C. Herry wrote the paper.

[6]These authors contributed equally to this work

[7]These authors contributed equally to this work

The authors declare they have no competing financial interests.

Europe PMC Funders Author Manuscripts

more recently between neuronal structures involved in the processing of emotions such as fear-related information[9-12]. Fear behaviour is known to depend on the interaction between the dorsal medial prefrontal cortex (dmPFC), and the basolateral amygdala (BLA) and recent data indicate that local or distant synchronization of neuronal activity within this dmPFC-BLA network strongly correlates with fear behaviour[9-12]. In particular, synchronization of spiking activity between dmPFC and BLA has been associated with resistance to extinction learning, whereas fear discrimination has been associated with transient, sensory-driven mPFC-BLA synchronization[10, 11]. However to date, the precise neuronal mechanisms mediating long-range network synchronization during fear behaviour remain unknown. Furthermore, a causal role of neuronal synchrony among dmPFC and BLA circuits in driving fear behaviour has not yet been demonstrated.

Results

Internally generated freezing behaviour

To address these questions, we performed single unit and local field potential (LFPs) recordings in the dmPFC and BLA of freely behaving mice submitted to auditory fear conditioning (Fig. 1a). Twenty-four hours following conditioning, re-exposure to the conditioned auditory stimulus (CS^+) but not to the control auditory stimulus (CS^-) induced conditioned freezing behaviour, which we used as readout of fear memory acquired upon associative learning (Fig. 1b). Interestingly, quantification of freezing episodes occurring inside or between CS^+ presentations indicated that mice froze more often between CS^+ presentations (Fig. 1c). Moreover, evaluation of freezing period onset distribution inside or between CS^+ presentations indicated that a large fraction of freezing periods (41.8 ± 0.03 %) was initiated outside of CS^+ presentations (Fig. 1d). Finally, cross-correlation analysis performed between freezing and CS^+ onset revealed that the latency of freezing period onset inside CS^+ presentations was delayed by approximately 1.5 second compared to CS^+ onset (Fig. 1e). These observations indicate, that in addition to freezing episodes driven by auditory inputs, internally generated mechanisms can maintain or initiate freezing episodes following CS^+ presentations.

dmPFC and BLA 4 Hz oscillations predict freezing behaviour

Analysis of dmPFC LFPs recorded throughout the behavioural sessions revealed a prominent and sustained 2-6 Hz oscillation with a peak frequency at 4 Hz (hereafter referred to as 4 Hz oscillations), which strongly correlated with episodes of freezing behaviour following conditioning (Fig. 2a-d and Supplementary Fig. 1a-b). Importantly, 4 Hz oscillations were not present when animals were passively immobile during the habituation session (Fig. 2a and Fig. 3a-c). Moreover, the duration and power of 4 Hz oscillations in the dmPFC was strongly correlated with the length of freezing episodes (Fig. 3d). To evaluate if 4 Hz oscillations could predict freezing behaviour, we first computed freezing-triggered spectrograms centered on the onset and offset of freezing episodes (Fig. 3e). Statistical analyses for the temporal progression of significant changes of 4 Hz power indicated that 4 Hz oscillations in the dmPFC emerge and terminate significantly earlier than freezing behaviour. These results strongly suggest that 4 Hz oscillations are an accurate predictor of freezing onset and offset, rather than a consequence of freezing behaviour. This observation

was further supported by additional analyses using supervised learning models, that allowed us to successfully predict freezing behaviour on a trial-by-trial basis using the 4 Hz dmPFC signal to noise ratio (SNR) (Fig. 3f-g**).** Importantly, 4 Hz oscillations developed during auditory fear conditioning (Supplementary Fig. 2), and dmPFC 4 Hz oscillations were also observed during freezing episodes in mice submitted to contextual fear conditioning indicating that 4 Hz oscillations might correspond to a general physiological signature of freezing behaviour (Supplementary Fig. 3). A similar but less prominent phenomenon was observed in the BLA, although the coupling between 4 Hz oscillations and freezing behaviour was stronger in the dmPFC, likely due to the different laminar anatomical organization of the two structures and putative localization of the source of the 4Hz oscillation in the prefrontal circuits. (Fig. 4 and Supplementary Fig. 1c-d and 4a-e). To evaluate if 4 Hz oscillations were the mere consequence of freezing-, motor-, or respiratory-related behaviour, we performed additional recordings in the ventrolateral periaqueductal grey (vlPAG), a neuronal structure involved in the genesis of freezing behavior and the control of breathing during emotional load[13-16]. Power spectrum analyses performed on vlPAG recordings failed to reveal significant 4 Hz oscillations during freezing episodes, which strongly suggests that 4 Hz oscillations do not reflect motor-, respiratory- or freezing-related activity (Supplementary Fig. 4f-g).

4 Hz oscillations are distinct from theta oscillations

To evaluate if dmPFC 4 Hz oscillations could correspond to hippocampal-dependent low theta oscillations observed previously during conditioned stimulus presentations[10, 12, 17, 18], we inactivated the medial septum (MS), a neuronal structure known to be involved in the genesis of theta oscillations[19]. Targeted, reversible, inactivation of the MS with muscimol, which is known to reduce theta power in the dorsal hippocampus[19], impaired dmPFC theta but had no effect on dmPFC 4 Hz oscillations (Supplementary Fig. 5a-e). In addition, this manipulation had no effects on the percentage of dmPFC neurons phase-locked to 4 Hz oscillations, but significantly reduced the number of dmPFC neurons phase-locked to theta oscillations (Supplementary Fig. 5f). Furthermore, in contrast to transient dmPFC local theta oscillations, which displayed CS^+-evoked phase resetting and were short-lasting (~300 ms)[9, 10], sustained dmPFC 4 Hz oscillations described in the present manuscript were not modulated by CS^+ presentations, did not display CS^+-evoked phase resetting (Supplementary Fig. 6), and could be maintained over long periods of freezing behaviour even between CS^+ presentations (Fig. 2a-b**,** Fig. 3d and Fig. 4a-b) suggesting that the two phenomena are generated independently. Together these data indicate that the development of hippocampus-independent, internally generated 4 Hz oscillations within dmPFC-BLA circuits temporally predict freezing behaviour.

dmPFC 4 Hz oscillations drive BLA during freezing

Interestingly, analyses of moment-to-moment covariations in oscillatory power and phase between structures revealed that during freezing episodes, 4 Hz oscillations in the dmPFC and BLA were strongly synchronized (Fig. 5a-b and Supplementary Fig. 7). Consequently, coherence between dmPFC and BLA LFPs was significantly enhanced during freezing behaviour (Fig. 5c and Supplementary Fig. 7). Moreover, a series of statistical directionality measures, in both the phase and the amplitude domain, revealed that dmPFC 4 Hz

oscillations lead BLA LFPs during freezing episodes but not during locomotor activity (Fig. 5b-d and Supplementary Fig. 7). Together, these data demonstrate that conditioned freezing behaviour is associated with a preferential dmPFC to BLA phase coupling of 4 Hz LFP oscillations.

4 Hz oscillations organize dmPFC and BLA firing activity

To evaluate the consequence of synchronized 4 Hz oscillatory activity on individual dmPFC and BLA putative excitatory principal neurons (PNs) ($n = 92$ and $n = 72$, respectively) and putative inhibitory interneurons (INs) ($n = 35$ and $n = 15$, respectively) (Supplementary Fig. 8), we measured the phase locking to dmPFC 4 Hz oscillations and changes in firing frequency of dmPFC and BLA neurons during fear behaviour. These analyses revealed that a large proportion of PNs and INs in both structures were significantly phase-locked to dmPFC 4 Hz oscillations during freezing episodes, among which the vast majority exhibited 4 Hz-related oscillatory activity (Fig. 6). Moreover, freezing episodes were associated with a global increase in the firing rate of PNs compared to no freezing periods in both the dmPFC and the BLA (Supplementary Fig. 8). Interestingly, correlation and co-firing analyses of pairwise spiking activity performed between neurons recorded in the dmPFC and neurons recorded in the BLA indicated that phase-locked pairs of PNs were significantly more co-activated during freezing episodes compared to both no freezing periods and non phase-locked neurons (Fig. 6c,h). Together, these data indicate that dmPFC and BLA PNs synchronize their firing activity to 4 Hz oscillations during freezing behaviour.

Optogenetic induction of dmPFC 4 Hz drives fear behaviour

To further evaluate the causal role of 4 Hz oscillations in synchronizing dmPFC-BLA PNs firing activity during fear behaviour, we artificially induced 4 Hz oscillations in the dmPFC of naïve animals by analog optogenetic modulation of dmPFC interneurons (INs), which contribute to the emergence of dmPFC 4 Hz oscillations (Supplementary Fig. 9). In particular, we manipulated parvalbumin-expressing INs, which is an efficient approach for inducing rhythmic inhibition of cortical PNs at low frequencies [20-22]. These genetically identified cells were predominantly phase-locked to 4 Hz oscillations and displayed 4 Hz oscillatory activity (Supplementary Fig. 9d-j). Rhythmically driving parvalbumin-expressing INs at 4 Hz, resulted in prominent 2-6 Hz oscillations in the dmPFC and induced persistent fear behaviour (Fig. 7a-c and Supplementary Fig. 10a-b). Importantly, freezing behaviour was frequency and structure specific as dmPFC rhythmic stimulation using a number of different control frequencies and BLA or motor cortex stimulation at 4 Hz were inefficient to induce fear responses (Fig. 7d-e and Supplementary Fig. 10c-d). Furthermore, we observed that the artificial induction of dmPFC 4 Hz oscillations synchronized dmPFC and BLA spiking activity during freezing episodes (Fig. 7f and Supplementary Fig. 10g-i). Given the emergence of 4Hz oscillations during fear conditioning and retrieval of contextual fear memory (Supplementary Fig. 2 and 3), we re-tested the mice 24 hours later in the context in which they received artificial induction of 4 Hz oscillations. Interestingly, in these conditions, mice exhibited contextual fear behaviour compared to GFP control animals (Fig. 7c and Supplementary Fig. 10a-b). Furthermore, mice exhibited low freezing levels when tested in a neutral context 24 hours later, indicating that fear behaviour was specific to the context where the optogenetic stimulation occurred (Supplementary Fig. 10b**).** Together,

these results indicate that freezing behaviour upon artificial induction of dmPFC 4 Hz oscillations cannot be explained by motor impairments and further suggest that 4 Hz oscillations are causally involved in the synchronization of dmPFC-BLA spiking activity and the expression of aversive fear memories. Finally, the post-training optogenetic silencing of BLA neurons during CS presentations significantly reduced fear behaviour indicating that the BLA is necessary for the full expression of conditioned fear behaviour (Supplementary Fig. 10e-f**).**

Discussion

In this study, we demonstrated that expression of conditioned fear memories is associated with prominent synchronous 4 Hz oscillations within dmPFC-BLA circuits, which organize the spiking activity of local neuronal populations. Furthermore, both dmPFC and BLA 4Hz oscillations develop specifically during fear conditioning and predict the onset and offset of freezing episodes. Moreover, the length of freezing episodes was also strongly correlated with the duration and power of dmPFC 4 Hz oscillations, a phenomenon not observed in the BLA. This is possibly due to the different laminar anatomical organization of the two structures. Indeed, aligned pyramidal cells in the cortex form spatially coherent dipoles. The resulting summation of field potentials allows the detection of high signal-to-noise ratio oscillations in the extracellular space[23]. The BLA on the other hand is a nuclear structure with no clear anatomical organization (dipoles are distributed uniformly and not aligned). Consequently, the SNR of extracellularly recorded LFP oscillations is expected to be lower than in the mPFC. Nonetheless, spike trains of a number of BLA neurons present both intrinsic 4Hz oscillations and phase locking to dmPFC 4Hz, whether it is in physiological conditions or during light stimulation. Moreover, the presence of 4 Hz oscillations in LFP is indicative of the underlying synaptic activity, however differences in the absolute power/SNR between the two structures cannot be interpreted as a stronger involvement of the dmPFC. Again, due to the radically different neuronal organization between the two structures, synaptic inputs are differentially filtered by the biophysical and topological properties of the BLA neural tissue[24, 25]. Importantly, our data indicate that internally generated freezing-related dmPFC 4 Hz oscillations constitute a specific oscillatory mechanism, distinct from CS^+-evoked dmPFC theta resetting observed previously[9, 10, 12]. These previously published studies[9, 10] evaluated transient sensory-evoked theta oscillations in the dmPFC, which lasted around 300 ms and have been linked to sensory-driven processes during fear behaviour, or fear discrimination[9, 10]. In striking contrast, the present 4 Hz oscillatory phenomenon correlated not only with long periods of freezing behaviour observed during CS^+ presentations, but also during spontaneously occurring freezing episodes. Functionally this implies that spontaneously occurring freezing periods are internally maintained or generated and not directly driven by sensory stimulations. To our knowledge, this is the first report of a sustained brain state (4 Hz oscillations) that predicts and temporally coincides with freezing episodes. The freezing responses observed between CS presentations are unlikely triggered by the context for several reasons. Firstly, it should be noted that mice are tested in a context distinct from the one used for the conditioning session. Secondly, freezing levels during CS^- presentations during retrieval were very low, indicating that the retrieval context was not aversive *per se* (Figure 1b, 13.19% freezing on

CS^{-} presentations). Our interpretation that freezing episodes occur between CS presentations relies on the induction of a fearful state after the initial CS-induced retrieval of the fear memory and thus the emergence of non-CS related spontaneous freezing episodes. Rather, our data and analyses suggest that the 4 Hz oscillations represent a mechanism for the initiation and maintenance of freezing episodes, inside and outside of CS presentations. Our present data also confirm published observations that CS^{+} onset is associated with a transient resetting of the phase of theta oscillations[9, 10], which is however specific for oscillations in the 8-12 Hz range and are associated with transient increases in theta power, but are not observed for the 4 Hz oscillations (Supplementary Fig. 6). Hence, these observations indicate that sustained 4 Hz oscillations described in the present manuscript do not correspond to sensory-driven transient theta oscillations previously observed[9, 10]. Altogether these results have important functional consequences as they indicate the existence of distinct and independent dmPFC neuronal oscillations involved in the regulation of different aspects of fear behaviour, such as stimulus-evoked attention processes related to the presentation of salient CS, fear discrimination, or to the expression of freezing behaviour. Importantly, all of these findings were observed in mice, additional studies are required to evaluate if these oscillations also occurs in different species.

Our data also indicate that stationary dmPFC 4 Hz oscillations do not correspond to hippocampus-mediated dmPFC theta oscillations observed previously[17] as muscimol inactivation of the medial septum, blocks hippocampal theta recorded in the dmFFC without affecting prefrontal 4 Hz oscillations, nor the percentage of dmPFC neurons phase-locked to 4 Hz oscillations. Our observation of BLA 4 Hz oscillatory activity during freezing behaviour is consistent with previous recordings of slow theta oscillations in the lateral amygdala during fear behaviour, which correlated with dorsal hippocampal theta oscillations[17, 18], although in these studies the temporal relation between CS^{+} onset, 4 Hz oscillatory activity, and freezing onset and offset was not clearly established. A recent observation of power increase for 4-7.5 Hz oscillations in the cingulate cortex in a hippocampus-dependent trace fear-conditioning paradigm is also partly consistent with our observation[26]. Indeed, the authors observed that in some conditioning trials, 4-7.5 Hz power increased during the interval separating the conditioned stimulus from the footshock. Although in this study, the neuronal interaction between the cingulate cortex and the BLA, the precise temporal relation between slow oscillation and freezing behaviour, and the causal role of prefrontal 4 Hz oscillations were not established. These data nevertheless suggest that prefrontal 4 Hz oscillations might be a general mechanism of fear expression encompassing classical auditory and contextual fear conditioning.

A key novel aspect of our study comes from the demonstration that during freezing behaviour, dmPFC 4 Hz oscillations entrain BLA oscillatory activity and synchronize spiking activity between dmPFC and BLA neurons. Recent publications have highlighted neuronal co-firing between prefrontal cortex and amygdala during resistance to extinction behaviour[11], LFP coherence between mPFC and BLA after CS^{+} onset during fear discrimination, and amygdala neurons phase-locked to dmPFC theta oscillations during fear discrimination[10]. To our knowledge, our data provide the first mechanistic demonstration of a 4 Hz-mediated long-range synchronization of spiking activity between dmPFC and BLA during freezing behaviour. Moreover, our findings also indicate that mPFC activity leads the

BLA one during freezing behaviour. Accordingly, we found that the optogenetic-mediated artificial induction of 4 Hz oscillations in dmPFC, synchronizes dmPFC and BLA neuronal activity and increases freezing behaviour in a persistent manner which is an unprecedented causal demonstration of the role of internally generated oscillations in driving behaviour. Indeed, neuronal synchronization between dmPFC and BLA has been classically evaluated using powerful correlational analyses[10, 11, 18], but never causally demonstrated. Our present data indicate that the genesis of 4 Hz oscillations in the dmPFC is sufficient to synchronize neuronal activity between mPFC and BLA and further drive the expression of freezing responses. Moreover, this effect was frequency and structure specific as dmPFC manipulation at other frequencies or 4 Hz induction in the motor cortex and BLA did not induce any behavioural effects. However, our data indicate that when freezing behaviour has been induced following auditory fear conditioning, the BLA was necessary for its full expression. Together these data strongly suggest that dmPFC 4 Hz oscillations are instrumental for dmPFC/BLA synchronization of neuronal activities during fear behaviour and that the synchronized firing activity of BLA neurons triggers fear responses (Supplementary Figure 11). It is important to note that the dmPFC 4 Hz analog optogenetic stimulation induced freezing behaviour during the stimulation but also 24 hours later in the context in which the mice were stimulated. This observation suggests that the artificial induction of dmPFC 4 Hz oscillations might be involved in the formation of associative fear memories. Another possibility could be that this artificial induction might lead to unspecific anxiety behavior. However, it is unlikely that a sudden inactivation or rhythmic inhibition of prefrontal areas could lead to unspecific anxiety behavior for at least two reasons. Published reports of optogenetic inactivation of the cingulate cortex during remote contextual memory retrieval, results in a reduction of contextual fear behaviour, an observation not consistent with a general increase in anxiety levels[27]. Furthermore, in our optogenetic experiments (Fig. 7), dmPFC 4 Hz induction induces freezing in a context specific manner, which is also an observation not consistent with a general increase in anxiety levels. Additionally, while it is possible that induction of 4 Hz oscillations lead to the formation of associative fear memories, an alternative interpretation is that contextual fear memory observed 24 hours following optogenetic stimulation is the direct consequence of the association between contextual elements and the aversive state induced by 4 Hz oscillations. This interpretation is consistent with the notion that dmPFC-BLA 4 Hz oscillations are causally involved in the expression of freezing behaviour.

Although, our data indicate that dmPFC 4 Hz oscillations are causally involved in the neuronal synchronization of spiking activity between dmPFC and BLA during freezing behavior, it is conceivable that this mechanism could be involved in other emotional processes such as avoidance, flight responses, sensory processes, or cognitive tasks. For instance recent data have observed 4 Hz oscillations in the whisker barrel cortex during respiration [28] and in the rat mPFC under working memory load during locomotor behaviour[29]. Another important aspect in the future will be also to identify the source of 4 Hz oscillations. Although our data indicate that these oscillations do not originate from the hippocampus and are localized in dmPFC circuits, additional work will be required in the future to address this question and unequivocally identify the source of 4 Hz oscillations. Ultimately, our data unravel a novel, specific 4 Hz oscillatory mechanism allowing the

expression of fear memories by long-range synchronization of neuronal activity between dmPFC and BLA neuronal circuits.

Methods

Animals

Naïve male C57BL6/J mice (3 months old, Janvier) and PV-IRES-Cre mice (3 months old, Jackson Laboratory, B6;129P2-Pvalb$^{tm1(cre)Arbr}$/J) were individually housed for at least 7 days before all experiments, under a 12-h light–dark cycle, and provided with food and water ad libitum. Experiments were performed during the light phase. All procedures were performed in accordance with standard ethical guidelines (European Communities Directive 86/60-EEC) and were approved by the committee on Animal Health and Care of Institut National de la Santé et de la Recherche Médicale and French Ministry of Agriculture and Forestry (authorization A3312001).

Behaviour

Auditory fear conditioning and testing took place in two different contexts (context A and B). The conditioning and testing boxes were cleaned with 70% ethanol and 1% acetic acid before and after each session, respectively. To score freezing behaviour independently of the experimenter, an automated infrared beam detection system located on the bottom of the experimental chambers was used (Coulbourn Instruments). Because the detection of our dependent variable (freezing) was independent of the experimenter, we did not use a blinding process for group allocation or behaviour scoring. The animals were considered to be freezing if no movement was detected for 2 s. On day 1, C57BL6/J mice were submitted to a habituation session in context A, in which they received four presentations of the CS^+ and of the CS^- (total CS duration, 30 s; consisting of 50-ms pips at 0.9 Hz repeated 27 times, 2 ms rise and fall, pip frequency, 7.5 kHz or white-noise, 80 dB sound pressure level).

Discriminative fear conditioning was performed on the same day by pairing the CS^+ with a US (1 s foot-shock, 0.6 mA, 5 CS^+–US pairings, inter-trial intervals, 20–180 s). The onset of the US coincided with the offset of the CS^+. The CS^- was presented after each CS^+–US association but was never reinforced (five CS^- presentations; inter-trial intervals, 20–180 s). The frequencies used for CS^+ and CS^- were counterbalanced across animals and randomization of CS^- and CS^+ allocation was performed using an online randomization algorithm (http://www.randomization.com).

On day 2, conditioned mice were submitted to a testing session (Retrieval session) in context B during which they received 4 and 12 presentations of the CS^- and CS^+, respectively. 13 naïve C57BL6/J mice recorded simultaneously in the dmPFC and BLA were included in this experiment and the data collected in two distinct replicates. Five additional naïve C57BL6/J mice recorded in the vlPAG were fear conditioned using the same protocol. Contextual fear conditioning took place in contexts A and B as describe above. On day 1, C57BL6/J mice were submitted for 5 min to a habituation session in context A. Contextual fear conditioning was performed 24 hours later by pairing context B with a US. The next day, mice were submitted for 12 min testing session (Retrieval) in context B. 6 naïve C57BL6/J mice were

included in this experiment and the data collected in two distinct replicates. For neck muscle EMG recordings, C57BL6/J mice were exposed to 20 CS^+ presentations in context B as describe above and auditory fear conditioning was performed on the same day by pairing the CS^+ with a US. 7 naïve C57BL6/J mice were included in this experiment and the data collected in two distinct replicates.

For optogenetic experiments using channelrhodopsin, PV-IRES-Cre mice (and GPF controls) were exposed on day 1 to context A as described above. During the session, four blue-light 4 Hz rhythmic analog (2 or 10 mW, 30 sec) stimulations were delivered in the dmPFC in order to activate parvalbumin-expressing interneurons. On day 2 and 3, mice were exposed to the same context as day 1, or to the neutral context B as described above without any stimulation, respectively. To test for the frequency and structure specificity of the stimulation, additional groups of naïve PV-IRES-Cre mice were submitted to four blue-light rhythmic analog dmPFC stimulations at different frequencies (1, 8, 10, and 12 Hz, stochastic 4 Hz composed of 2-12 Hz frequency with an average at 4 Hz, 10 mW, 30 sec, $n = 6$ mice) or to four blue-light rhythmic analog stimulations at 4 Hz of the motor cortex ($n = 4$ mice) or the BLA ($n = 5$ mice). These 5 mice infected in the BLA were also submitted to auditory fear conditioning as described above and tested 24 and 48 hrs later to evaluate the effect of BLA silencing during fear behaviour. Randomization of group allocation (ChR2 versus GFP controls) was performed using an online randomization algorithm (http://www.randomization.com).

For pharmacological experiments, C57BL6/J mice were submitted to a fear conditioning paradigm consisting of CS^+ and US pairings in context A as described above. On days 2, 3, and 4, conditioned mice were tested in context B, during which they received four presentations of the CS^+ before muscimol injections (Day 2, Test 1), 5 min after muscimol injections (Day 3, Inac.), and 24 hours following muscimol injections (Day 4, Test 2). 6 naïve C57BL6/J mice were included in this experiment and the data collected in two distinct replicates.

Surgery and recordings

Mice were anaesthetized with isoflurane (induction 3%, maintenance 1.5%) in O_2. Body temperature was maintained at 37 °C with a temperature controller system (FHC). Mice were secured in a stereotaxic frame and unilaterally implanted in the left dorsomedial prefrontal cortex (dmPFC) with a multi-wire electrode array aimed at the following coordinates: 2.0 mm anterior to the bregma; 0.3 mm lateral to the midline; and 0.8 to 1.4 mm ventral to the cortical surface and in the left basolateral amygdala (BLA) with a multi-wire electrode array aimed at the following coordinates: 1.7 mm posterior to the bregma; 3 mm lateral to the midline; and 4 mm ventral to the cortical surface.

An additional group of mice was only implanted in the ventrolateral periaqueductal gray at the following coordinates: −4.30 mm anterior to the bregma, 0.55 mm lateral to the midline; and 2.20 mm ventral to the cortical surface. For contextual fear conditioning experiments, mice were only implanted in the dmPFC. For electromyographic (EMG) recording experiments, Teflon-coated stainless steel electrodes (AM systems) were sutured in the right

and left nuchal muscles. Wires were connected to a multi-wire electrode array connector attached to the skull.

For pharmacological experiments, animals were implanted in the dmPFC as the same coordinate as above and in dorsal hippocampus (dHip) at the following coordinates: 2 mm posterior to bregma; 1.2 mm lateral to midline; and 1.2 to 1.4 mm ventral to the cortical surface. The electrodes consisted of 16 individually insulated nichrome wires (13 μm inner diameter, impedance 30–100 KΩ; Kanthal) contained in a 26-gauge stainless-steel guide cannula. The wires were attached to an 18-pin connector (Omnetics) and two connectors were used for each mouse. All implants were secured using Super-Bond cement (Sun Medical). After surgery mice were allowed to recover for 7 days and were habituated to handling. Analgesia was applied before, and 1 day after surgery (Metacam, Boehringer). Electrodes were connected to a headstage (Plexon) containing sixteen unity-gain operational amplifiers. The headstage was connected to a 16-channel preamplifier (gain 100× bandpass filter from 150 Hz to 9 kHz for unit activity, Plexon). Spiking activity was digitized at 40 kHz and bandpass filtered from 250 Hz to 8 kHz, and isolated by time-amplitude window discrimination and template matching using a Multichannel Acquisition Processor system (Plexon). At the conclusion of the experiment, recording sites were marked with electrolytic lesions before perfusion, and electrode tip locations were reconstructed with standard histological techniques.

Single-unit analyses

Single-unit spike sorting was performed using Off-Line Spike Sorter (OFSS, Plexon) for all behavioural sessions. Principal-component scores were calculated for unsorted waveforms and plotted in a three-dimensional principal-component space; clusters containing similar valid waveforms were manually defined. A group of waveforms were considered to be generated from a single neuron if the waveforms formed a discrete, isolated, cluster in the principal-component space and did not contain a refractory period less than 1 ms, as assessed using auto-correlogram analyses. To avoid analysis of the same neuron recorded on different channels, we computed cross-correlation histograms. If a target neuron presented a peak of activity at a time that the reference neuron fired, only one of the two neurons was considered for further analysis.

To separate putative inhibitory interneurons (INs) from putative excitatory principal neurons (PNs) we used an unsupervised clustering algorithm based on Ward’s method. In brief, the Euclidian distance was calculated between all neuron pairs based on the three-dimensional space defined by each neuron’s average half-spike width (measured from trough to peak), the firing rate, and the area under the hyperpolarization phase of the spike. An iterative agglomerative procedure was then used to combine neurons into groups based on the matrix of distances such that the total number of groups was reduced to give the smallest possible increase within-group sum of square deviation.

For the detection of interactions between units recorded in the dmPFC and BLA, the spike trains of each simultaneously recorded pair were binned (10 ms bin size), the cross-correlation of the binned histograms was calculated over multiple lags (maximum lag: ± 500 ms) and the peak cross-correlation coefficient for each pair was determined. For the

detection of co-firing property for unit pairs, spike trains were binned as before and the co-firing index was calculated as the ratio of co-occurring (common) spikes to the total number of spikes for the two units. This provides a simple, yet direct, measure of the co-occurrence of unit spikes on multiple levels of temporal resolution. For the determination of the bin-size and the robustness of the method, different bin sizes were tested and they all gave qualitatively similar results. Among those tested, 10 ms was selected since it allows the identification of potentially monosynaptic interactions. To evaluate if neurons were oscillating at 4 Hz we used Gabor functions which are commonly used to fit autocorrelation (AC) histograms of non-stationary rhythmic biological time series such as neuronal spiking activity[30-32]. Gabor functions are damped sine waves with two components, first the sine wave frequency (f_o), the amplitude of which is modulated by the second term, here the damping frequency (f_d). The Gabor functions served as predicted AC (pAC), used to fit the actual AC of the frequencies of interest. We constructed a set of Gabor functions as follows[32]:

$$pAC_{fofd}=cos\left(2\pi * x * fo\right) * exp\left(C * x^2 * fd\right)$$

,with f_o and f_d both ranging from 1 to 25 Hz, hence creating 100 × 100 predicted AC. The quality of the fit of each predicted AC was then assessed by its correlation (Spearman's ρ) with the actual AC of specific frequency bands (calculated for lags t of 0–500 ms), and this correlation score was plotted for each f_0, f_d pair. Points showing the highest correlation thus represent candidate f_0, f_d pairs capable of predicting oscillations.

Local field potential and EMG analyses

Local field potentials were analysed using custom-written Matlab programs. Raw LFP traces were filtered between 0.7 Hz and 400 Hz and downsampled to 1 kHz. All signals were filtered using zero-phase distortion 6th order Butterworth filters. For phase analyses, the signal was filtered in the desired frequency band (2 - 6 Hz for the 4Hz oscillation) and the complex valued analytic signal was calculated using the Hilbert transform as below.

$$\rho\left(t\right)e^{-i\varphi(t)}$$

The vector length and the arctangent of the vector angle provide the estimation of the instantaneous amplitude and instantaneous phase of the signal respectively at every time point. All analyses were performed during freezing episodes and, where indicated, during subsampled non-freezing epochs. A phase of 0° corresponds to the peak of prefrontal - amygdala oscillations. LFP power spectrum and LFP-LFP coherence estimations were, unless otherwise noted, performed using the multitaper method[33]. Briefly, data was multiplied by a set of 2-5 orthogonal taper functions (discrete prolate spheroidal sequences), Fourier transformed using window size of two seconds and averaged to obtain a direct multitaper spectral estimate.

Signal to noise ratio (SNR) for 4 Hz power was calculated as the ratio of the mean power in the 2-6 Hz band to the mean power outside of this band. Because, one mouse didn’t show

immobility behaviour during habituation, it was excluded from SNR analyses. For coherence analyses, a method based on imaginary coherence was employed[34]. Imaginary coherence was calculated as $$iCoh = \frac{|Im(\Sigma_{bins} S_{xy})|}{\sqrt{\Sigma_{bins}(S_{xx}) * \Sigma_{bins}(S_{yy})}},$$ where Sxy is the cross-spectrum, Sxx and Syy the auto-spectra and summation takes place over the spectrogram bins corresponding to the quantified state. By keeping the imaginary part of the normalized cross-spectrum, coherence value is weighted inversely proportional to the time lag between the two signals. Consequently, it is sensitive only to time-lagged signals, whereas the effect of absolutely synchronous signals is eliminated. Given the very synchronous nature of the oscillation examined here and the small phase lag, it is expected that imaginary coherence is under-estimating the strength of the interaction. However, we opted for this conservative flavor of coherence analysis, in order to avoid any influence of volume conducted currents or artifacts that can artificially boost coherence values.

To investigate any potential causal interaction between the oscillations recorded in the two structures, spectrally resolved Granger causality was calculated for the unfiltered LFP signals. Granger causality is a statistical measure of the predictive power of one variable over another. Linear trends were removed from the LFP signals and signals were normalized before the analysis. For these analyses, the MVGC multivariate Granger causality toolbox [35] was used to fit a higher order vector autoregressive model to the processes. Data was tested for stability in time and model order was determined using the Akaike Information Criterion (AIC). To identify directionality and quantify the lag between the two signals in terms of phase and amplitude, a point-process was defined consisting of the peaks of the bandpass filtered LFP signal for each of the two structures. The lag of the peak of the cross-correlation of these point-processes identifies the time lag of the oscillation in the two structures and the directionality of their potential interaction. To avoid any potential bias due to phase asymmetry, the same procedure was tested for the troughs giving identical results. To investigate this relationship throughout the oscillation cycle, the phase of each analytical signal was extracted using the Hilbert transform and the distribution of the phase differences between the two structures was characterized for deviation from uniformity using circular statistics and Monte Carlo simulations. To evaluate the specific role of phase, amplitude and their interplay on the directionality and causality measures for the LFP data, a procedure was devised for the selective perturbation of phase and amplitude of the signals. Signals were converted in the spectral domain using a discrete Fourier transform and the phase (or amplitude) component of the signal was permuted, leaving the amplitude (or phase) intact. The modified signal was converted back to the time domain using the inverse Fourier transform. For the power comodulation analysis, the power profile for each frequency bin in each structure was calculated and the correlation coefficient of every pair was calculated[36].

To compare the impact of CS^+ during freezing on local theta and 4 Hz phase resetting we used a multitaper analysis of LFP signals for frequencies ranging from 2 to 12 Hz and computed a stimulus-triggered spectrogram. For the CS^+-triggered theta and 4Hz phase overlays, signals were filtered in the corresponding range (theta: 8-12 Hz; 4Hz: 2-6Hz) and phases were extracted from the analytic signal as described above. To quantify phase

Europe PMC Funders Author Manuscripts

stability across all CS^+ pip during freezing episodes we calculated the mean resultant length (MRL) for all time-frequency pairs. To evaluate the predictive value of 4 Hz power on freezing behaviour, we used wavelet analysis, that in some instances allows a higher temporal resolution, to quantify the spectral content of the signal for frequencies between 2 to 12 Hz and computed freezing-triggered spectrograms. To evaluate the latency to freeze in response to the CS^+, individual tone onsets and freezing period onsets for individual mice were binned (100 ms bin size), smoothed and averaged and cross-correlation analysis was performed on these data taking freezing onset epochs as the reference event (Fig.1e). In these conditions negative lags indicate the precedence of freezing events by conditioned stimuli. Statistical significance was evaluated using two different approaches and then combined. We first simulated 1000 instances of a uniform distribution of freezing episodes and recomputed the cross-correlation analysis. We next shuffled 1000 times the freezing ISIs of the actual freezing episodes to preserve the first order statistics of freezing behavior but perturb its relation to CS^+ and recomputed the cross-correlation analysis. The results of both analyses were averaged to produce a more robust significance threshold. However, each individual result was not qualitatively and quantitatively different from the final average. One interesting characteristic of the cross-correlation is its oscillatory nature, which is due to the rhythmic repetition of CS^+ (27 pips delivered at 1.1 Hz) and the tendency of elicited freezing to occur in response to these events (Fig. 1e).

For correlation analyses between freezing behaviour and 4 Hz oscillations (Fig. 3d and Supplementary Fig. 2), we first evaluated the percentage of time individual animals were freezing during the entire recording session. For 4 Hz quantification, 4 Hz oscillation periods were evaluated as periods of significant 4 Hz SNR, as compared to baseline (a 2 min period before the first CS presentation). 4 Hz expressed as the percentage of total time corresponds to the ratio of the total duration of 4 Hz episodes to the recording session duration. For electromyographic recordings, unilateral EMG signals were band pass filtered (100-1000 Hz), rectified and integrated (convolution with 100ms Gaussian kernel). Delta EMG signal was calculated as the differential EMG recorded in the left and right nuchal muscle [37]. The absolute value of Delta EMG was then Z-scored transformed and averaged around freezing onsets (−500ms to 500ms) occurring during CS^+ presentation, both during Habituation and fear conditioning.

Phase locking analyses

For phase modulation analysis, the variance-stabilized ln(Z) ($Z = R^2/n$, R being the resultant length and n the sample size) statistics for the Rayleigh test for uniformity against the von Mises distribution were calculated [38, 39]. To partially account for the sample size bias of the resultant length, only units with at least 100 spikes during freezing behaviour were taken into consideration. All results were corroborated using the pairwise phase consistency method, a bias-free estimate of neuronal synchronization based on the average pairwise circular distance

$$D=\frac{2}{N\,(N-1)}\sum_{i=1}^{N-1}\sum_{j=(i+1)}^{N}|\theta_i-\theta_j|\;mod\;\pi,$$

with θ_i and θ_j being the phases from two different spikes. This method is analytically equivalent to the squared phase locking value[40]. To calculate the statistics for each unit, bootstrap analyses and Monte Carlo simulations were performed. In the Monte Carlo simulations, the Y_{sim} value, indicating the expected value for a uniform prior distribution, was calculated for each sample size. Units for which the Y_{unit} was exceeding the 95% percentile of the simulated Y_{sim} estimate, were considered phase locked. For the bootstrap statistics, in order to take into account the higher-order statistics of the spike trains, for each unit, the inter-spike intervals were shuffled randomly and the potentially not uniform prior distribution was calculated.

Phases for both mPFC and BLA spikes were extracted using the mPFC 4Hz oscillation phase that exhibits the highest SNR and allows for direct comparison of the phase locking statistics. For the statistical evaluations, before the phase extraction, the prior distribution of phases of the 4 Hz oscillation was examined, and as is the case for other neuronal slow oscillations, this prior distribution deviates from the uniform distribution. This bias can alter the phase locking statistics and produce false positives[38, 39]. To account for this potential bias, the phases of the LFPs were transformed using the inverse of the empirical cumulative density function to return a signal with uniform prior distribution. Following this transformation, the spike phases are drawn from a uniform distribution allowing the application of the circular statistics for detecting deviations from uniformity. For normalized averaged phase density analyses, the circular histogram for each neuron was normalized to the maximum and the averaged circular histogram was computed.

Supervised learning algorithms

To establish the predictive value of dmPFC and BLA 4 Hz oscillations on the animal's behavioural state ("freezing" or "not freezing"), we used two distinct machine learning approaches. Specifically, we used the 4 Hz signal-to-noise ratio (SNR) of the two structures as features to train a naïve Bayes classifier and a Support Vector Machine (SVM). Based on the time-resolved spectral decomposition of the signals (spectrograms), we calculated the mean 4 Hz SNR across three consecutive time bins (with a bin size of 150 ms) and we assigned a binary value based on the behavioral state of the animal during the corresponding time (450 ms: freezing= 1; mobility = 0). Each formed SNR-binary value pair constitutes a single data point used as an input to the classifier.

For this analysis we considered the total duration of the recordings, that is, all time bins were used in this analysis. SVM projects data into a higher-dimensional space and estimates a hyperplane that best separates the data points belonging to distinct classes[41]. Naïve Bayes classifiers assume independence of the probability distributions of the features and classify the test data based on the maximal posterior probability of class assignment[42]. The dataset was randomly split into a training dataset containing 70% of the data points, which was used to train the classifiers, and a test dataset containing the remaining 30% of data points that were used to test the accuracy of the algorithms. In order to estimate the stability of the algorithms and confidence intervals of the accuracy and receiver operating characteristic (ROC) curves of the classifiers, we implemented a Monte-Carlo procedure, whereby the

dataset was randomly split 1000 times in mutually exclusive training and test datasets and the algorithms were trained and tested on the respective datasets. The accuracy, defined as:

$$accuracy = \frac{\#true\ positives + \#true\ negatives}{\#datapoints},$$

and the area under the curve (AUC) of the ROC curve were used to characterize the performance of the classifiers and were compared with the same algorithms trained on shuffled data using the exact same Monte-Carlo procedure.

Statistical analyses

For each statistical analysis provided in the manuscript, the Kolmogorov–Smirnov normality test was first performed on the data to determine whether parametric or non-parametric tests were required. When multiple statistical tests were performed, Bonferroni corrections were applied. Two different approaches were used to calculate the sample size. For studies in which we had sufficient information on response variables, power analyses were carried out to determine the number of mice needed. For studies in which the behavioural effect of the manipulation could not be pre-specified, such as optogenetic experiments, we used a sequential stopping rule (SSR). In essence this method enables null-hypothesis tests to be used in sequential stages, by analysing the data at several experimental points using *t*-tests. Usually the experiment started by testing only a few animals and if the *P* value was below 0.05, the investigator declared the effect significant and stopped testing. If the *P* value was greater than 0.36, the investigator stopped the experiment and retained the null hypothesis.

For sample-size estimation using power analyses, we used an on-line power analysis calculator (G*Power3). For each analysis, sample size was determined using a power > 0.9 and alpha error = 0.05. All tests were two-sided. Power analyses were computed for matched pairs (cued and contextual fear conditioning protocol (Fig. 1 and Supplementary Fig. 4) and pharmacological experiments (Supplementary Fig. 5)). In our behavioural experiments, a critical parameter is freezing level, and the numerical endpoint typically ranges between 50 and 70% freezing for CS^+ presentations immediately following auditory fear conditioning and between 10 and 30% freezing for CS^- presentations. A minimum biologically significant difference in the mean values between CS^- and CS^+ conditions for cued fear conditioning (Fig. 1) or between habituation and test sessions for contextual fear conditioning (Supplementary Fig. 4), is 1.5-fold. If we assume a standard deviation of 1.5 for a mean value of 60% freezing for CS^+ test session and 20% freezing for CS^- habituation (which are realistic numbers), then a minimum $n = 6$ is needed to reject the null hypothesis with 90% probability. Sample size determination using SSRs analyses was used for optogenetic experiments in which it was not possible to determine a priori the effect of the optical manipulation. We used *P* values of 0.05 and 0.36 for lower and upper criterion.

Muscimol inactivation

Mice were unilaterally implanted with stainless steel guide cannula (26 gauge; Plastics One) aimed at the MS using an angle of 10° and recording electrodes were implanted in the dmPFC and the dHip as described in the “Surgery and recordings” methodological section.

To target the MS, we used the following coordinates: 1 mm anterior to bregma; 0.7 mm lateral to midline and 3.0 to 3.3 mm ventral to the cortical surface with an angle of 10° in the coronal plane. The cannula was secured using Super-Bond cement (Sun Medical). On the injection day, muscimol (Muscimol-Bodipy-TMR-X conjugate, Invitrogen; 0.8 mM in PBS 0.1 M) was infused at a rate of 0.2 μL/min during 2 min (total volume of 0.4 μL). On the injection day, muscimol was infused 15 min before the behavioural test. After the end of the experiment, muscimol was again infused with the same parameters to control for the drug diffusion within the MS and mice were perfused. Brains were collected for histological analyses as described below.

Anatomical analysis

Mice were euthanized with isoflurane and perfused through the left ventricle with 4% w/v paraformaldehyde (PFA) in 0.1 M PBS. Brains were dissected out and postfixed for 24 h at 4 °C in the same solution. 60μm-thick sections were cut, mounted on gelatin-coated microscope slides, and dried. Sections were stained with toluidine blue, dehydrated and mounted. Electrolytic lesions were identified with conventional transmission light microscopy. Only recordings with confirmed lesions in cingulate/ prelimbic areas of dmPFC and basolateral amygdala (BLA) were included in our analyses. For verification of muscimol (MUS) injections in the medial septum (MS) and viral injections in dmPFC, BLA or motor cortex, serial 80 μm-thick slices were imaged using an epifluorescence system (Leica DM 5000) fitted with a 10× dry objective. The location and the extent of the injections/infections were visually controlled. All included MUS injections were targeted and limited to the MS. Similarly, only infections accurately targeting the region of interest were considered for behavioural and electrophysiological analyses.

Virus injections and optogenetics

For optical identification of parvalbumin-expressing interneurons, conditional AAV encoding ChR2 (AAV-EF1a-DIO-hChR2(H134R)-EYFP, serotype 5, Vector Core, University of North Carolina) or ArchT (AAV-FLEX-ArchT-GFP, serotype 5, Vector Core, University of North Carolina) were bilaterally injected into the dmPFC of PV-IRES-Cre mice (n = 12 mice) from glass pipettes (tip diameter 10-20 μm) connected to a Picospritzer (Parker Hannifin Corporation; approximately 0.4 μL per hemisphere) at the following coordinates : dmPFC: 2.0 mm anterior to bregma; 0.4 mm lateral to midline and 0.9 to 1.2 mm ventral to the cortical surface. 1-2 weeks after the injection mice were implanted bilaterally with optic fibers (diameter: 200 μm; numerical aperture: 0.37; flat tip; Doric Lenses) at the same coordinates. All implants were secured using Super-Bond cement (Sun Medical). For experiments using optogenetic stimulation coupled to single unit and LFP recordings, one of the two optic fibers was combined to the array of 16 or 32 individually insulated nichrome wires. Single unit recordings during the manipulation of PV INs were performed as described in the “Surgery and recordings” section.

Behavioural and recording experiments were performed 3-5 weeks post-injection. The light (approximately 2 or 10 mW per implanted fiber) was bilaterally conducted from the laser (OptoDuet 473/593 nm, Ikecool) to the mice via two fiber-optic patch cords (diameter: 200 μm, Doric Lenses), connected to a rotary joint (1×2 fiber-optic rotary joint, Doric Lenses)

that allowed mice to freely move in the behavioural apparatus. For optical control of parvalbumin-expressing interneurons, conditional AAV encoding ChR2 (AAV-EF1a-DIO-hChR2(H134R)-EYFP, serotype 5, Vector Core, University of North Carolina) were bilaterally injected into the dmPFC or the BLA at the same coordinates as above or into the motor cortex of PV-IRES-Cre mice at the following coordinates : motor cortex: 2.0 mm anterior to bregma; 1.5 mm lateral to midline and 1.3 mm ventral to the cortical surface. Control experiments were performed using an AAV containing the DNA construct for only GFP (AAV-FLEX-GFP, Vector Core, University of North Carolina).

For optogenetic manipulation of PV INs during behaviour, we used a 30 sec analog dmPFC stimulation delivered at 1, 4, 8, 10, or 12 Hz. As a control we also used a stochastic 4 Hz analog dmPFC stimulation generated by an oscillator with a randomly time-modulated frequency drawn from a Gaussian distribution centered on 4Hz. The power spectrum of the signal displayed a broad peak around 4Hz but the duration of each cycle varied randomly from 0.15 to 0.6 sec, therefore destroying the regularity of the population activity. For motor cortex experiments, we used a 4 Hz analog stimulation. For BLA silencing experiments, a continuous pulse of blue light was applied during CS^+ presentations 24 hrs following fear conditioning. After behavioural and recording experiments, mice were perfused and histological analysis was performed. A Supplementary Methods checklist is available.

Supplementary Material

Refer to Web version on PubMed Central for supplementary material.

Aknowledgements

We thank the members of the Herry laboratory for helpful discussions and comments on the manuscript and K. Deisseroth and E. Boyden for generously sharing material. This work was supported by grants from the French National Research Agency (ANR-2010-BLAN-1442-01; ANR-10-EQPX-08 OPTOPATH; LABEX BRAIN ANR 10-LABX-43, LABEX TRAIL ANR 10-LABX-57), the European Research Council (ERC) under the European Union's Seventh Framework Program (FP7/2007-2013)/ERC grant agreement no. 281168, the Conseil Regional d'Aquitaine (C.H.), the Fondation pour la Recherche Médicale (FRM) (F.C.), the CNRS ATIP program (2014) and the city of Paris (Grant Emergence 2014), the French National Research Agency (ANR—10—LABX—54 MEMO LIFE ANR—11—IDEX—0001—02 PSL) (K.B.), Munich Cluster for Systems Neurology (SyNergy, EXC 1010), DFG Priority Program 1665 and 1392 and BMBF via Grant no. 01GQ0440 (BCCN Munich) (A.S.) and scholarship from the Erasmus Mundus program Neurasmus (N.K.).

References

1. Bosman CA, et al. Attentional stimulus selection through selective synchronization between monkey visual areas. Neuron. 2012; 75:875–888. [PubMed: 22958827]
2. Siegel M, Donner TH, Oostenveld R, Fries P, Engel AK. Neuronal synchronization along the dorsal visual pathway reflects the focus of spatial attention. Neuron. 2008; 60:709–719. [PubMed: 19038226]
3. Rodriguez E, et al. Perception's shadow: long-distance synchronization of human brain activity. Nature. 1999; 397:430–433. [PubMed: 9989408]
4. Hipp JF, Engel AK, Siegel M. Oscillatory synchronization in large-scale cortical networks predicts perception. Neuron. 2011; 69:387–396. [PubMed: 21262474]
5. Friedrich RW, Habermann CJ, Laurent G. Multiplexing using synchrony in the zebrafish olfactory bulb. Nature neuroscience. 2004; 7:862–871. [PubMed: 15273692]
6. Riehle A, Grun S, Diesmann M, Aertsen A. Spike synchronization and rate modulation differentially involved in motor cortical function. Science. 1997; 278:1950–1953. [PubMed: 9395398]

7. Benchenane K, et al. Coherent theta oscillations and reorganization of spike timing in the hippocampal- prefrontal network upon learning. Neuron. 2010; 66:921–936. [PubMed: 20620877]
8. Gregoriou GG, Gotts SJ, Zhou H, Desimone R. High-frequency, long-range coupling between prefrontal and visual cortex during attention. Science. 2009; 324:1207–1210. [PubMed: 19478185]
9. Courtin J, et al. Prefrontal parvalbumin interneurons shape neuronal activity to drive fear expression. Nature. 2014; 505:92–96. [PubMed: 24256726]
10. Likhtik E, Stujenske JM, Topiwala MA, Harris AZ, Gordon JA. Prefrontal entrainment of amygdala activity signals safety in learned fear and innate anxiety. Nature neuroscience. 2014; 17:106–113. [PubMed: 24241397]
11. Livneh U, Paz R. Amygdala-prefrontal synchronization underlies resistance to extinction of aversive memories. Neuron. 2012; 75:133–142. [PubMed: 22794267]
12. Stujenske JM, Likhtik E, Topiwala MA, Gordon JA. Fear and safety engage competing patterns of theta-gamma coupling in the basolateral amygdala. Neuron. 2014; 83:919–933. [PubMed: 25144877]
13. Gabbott PL, Warner TA, Jays PR, Salway P, Busby SJ. Prefrontal cortex in the rat: projections to subcortical autonomic, motor, and limbic centers. J Comp Neurol. 2005; 492:145–177. [PubMed: 16196030]
14. Holstege G. The periaqueductal gray controls brainstem emotional motor systems including respiration. Progress in brain research. 2014; 209:379–405. [PubMed: 24746059]
15. Subramanian HH, Balnave RJ, Holstege G. The midbrain periaqueductal gray control of respiration. The Journal of neuroscience : the official journal of the Society for Neuroscience. 2008; 28:12274–12283. [PubMed: 19020021]
16. Vianna DM, Landeira-Fernandez J, Brandao ML. Dorsolateral and ventral regions of the periaqueductal gray matter are involved in distinct types of fear. Neurosci Biobehav Rev. 2001; 25:711–719. [PubMed: 11801296]
17. Lesting J, et al. Patterns of coupled theta activity in amygdala-hippocampal-prefrontal cortical circuits during fear extinction. PloS one. 2011; 6:e21714. [PubMed: 21738775]
18. Seidenbecher T, Laxmi TR, Stork O, Pape HC. Amygdalar and hippocampal theta rhythm synchronization during fear memory retrieval. Science. 2003; 301:846–850. [PubMed: 12907806]
19. Yoder RM, Pang KC. Involvement of GABAergic and cholinergic medial septal neurons in hippocampal theta rhythm. Hippocampus. 2005; 15:381–392. [PubMed: 15630696]
20. Stark E, et al. Inhibition-induced theta resonance in cortical circuits. Neuron. 2013; 80:1263–1276. [PubMed: 24314731]
21. Siegle JH, Wilson MA. Enhancement of encoding and retrieval functions through theta phase-specific manipulation of hippocampus. Elife. 2014; 3:e03061. [PubMed: 25073927]
22. Atallah BV, Bruns W, Carandini M, Scanziani M. Parvalbumin-expressing interneurons linearly transform cortical responses to visual stimuli. Neuron. 2012; 73:159–170. [PubMed: 22243754]
23. Nunez, PL.; Srinivasan, R. Electric fields of the brain: the neurophysics of EEG. Oxford University Press; 2006. second edition
24. Magee JC. Dendritic integration of excitatory synaptic input. Nature reviews. Neuroscience. 2000; 1:181–190. [PubMed: 11257906]
25. Vaidya SP, Johnston D. Temporal synchrony and gamma-to-theta power conversion in the dendrites of CA1 pyramidal neurons. Nature neuroscience. 2013; 16:1812–1820. [PubMed: 24185428]
26. Steenland HW, Li XY, Zhuo M. Predicting aversive events and terminating fear in the mouse anterior cingulate cortex during trace fear conditioning. The Journal of neuroscience : the official journal of the Society for Neuroscience. 2012; 32:1082–1095. [PubMed: 22262906]
27. Goshen I, et al. Dynamics of retrieval strategies for remote memories. Cell. 2011; 147:678–689. [PubMed: 22019004]
28. Ito J, et al. Whisker barrel cortex delta oscillations and gamma power in the awake mouse are linked to respiration. Nature communications. 2014; 5:3572.
29. Fujisawa S, Buzsaki G. A 4 Hz oscillation adaptively synchronizes prefrontal, VTA, and hippocampal activities. Neuron. 2011; 72:153–165. [PubMed: 21982376]

Europe PMC Funders Author Manuscripts

Methods References

30. Engel AK, Konig P, Gray CM, Singer W. Stimulus-Dependent Neuronal Oscillations in Cat Visual Cortex: Inter-Columnar Interaction as Determined by Cross-Correlation Analysis. The European journal of neuroscience. 1990; 2:588–606. [PubMed: 12106294]
31. Gray CM, Konig P, Engel AK, Singer W. Oscillatory responses in cat visual cortex exhibit inter-columnar synchronization which reflects global stimulus properties. Nature. 1989; 338:334–337. [PubMed: 2922061]
32. Young MP, Tanaka K, Yamane S. On oscillating neuronal responses in the visual cortex of the monkey. Journal of neurophysiology. 1992; 67:1464–1474. [PubMed: 1629758]
33. Mitra PP, Pesaran B. Analysis of dynamic brain imaging data. Biophys J. 1999; 76:691–708. [PubMed: 9929474]
34. Nolte G, et al. Identifying true brain interaction from EEG data using the imaginary part of coherency. Clinical neurophysiology : official journal of the International Federation of Clinical Neurophysiology. 2004; 115:2292–2307. [PubMed: 15351371]
35. Barnett L, Seth AK. The MVGC multivariate Granger causality toolbox: a new approach to Granger-causal inference. Journal of neuroscience methods. 2014; 223:50–68. [PubMed: 24200508]
36. Buzsaki G, et al. Hippocampal network patterns of activity in the mouse. Neuroscience. 2003; 116:201–211. [PubMed: 12535953]
37. Steenland HW, Zhuo M. Neck electromyography is an effective measure of fear behavior. Journal of neuroscience methods. 2009; 177:355–360. [PubMed: 19010352]
38. Siapas AG, Lubenov EV, Wilson MA. Prefrontal phase locking to hippocampal theta oscillations. Neuron. 2005; 46:141–151. [PubMed: 15820700]
39. Sirota A, et al. Entrainment of neocortical neurons and gamma oscillations by the hippocampal theta rhythm. Neuron. 2008; 60:683–697. [PubMed: 19038224]
40. Vinck M, van Wingerden M, Womelsdorf T, Fries P, Pennartz CM. The pairwise phase consistency: a bias-free measure of rhythmic neuronal synchronization. Neuroimage. 2010; 51:112–122. [PubMed: 20114076]
41. Cortes C, V V. Support-vector networks. Mach. Learn. 1995; 20:273–297.
42. Bishop, CM. Pattern Recognition and Machine Learning *Information Science and Statistics*. Springer-Verlag New York, Inc.; Secaucus, NJ, USA: 2006.

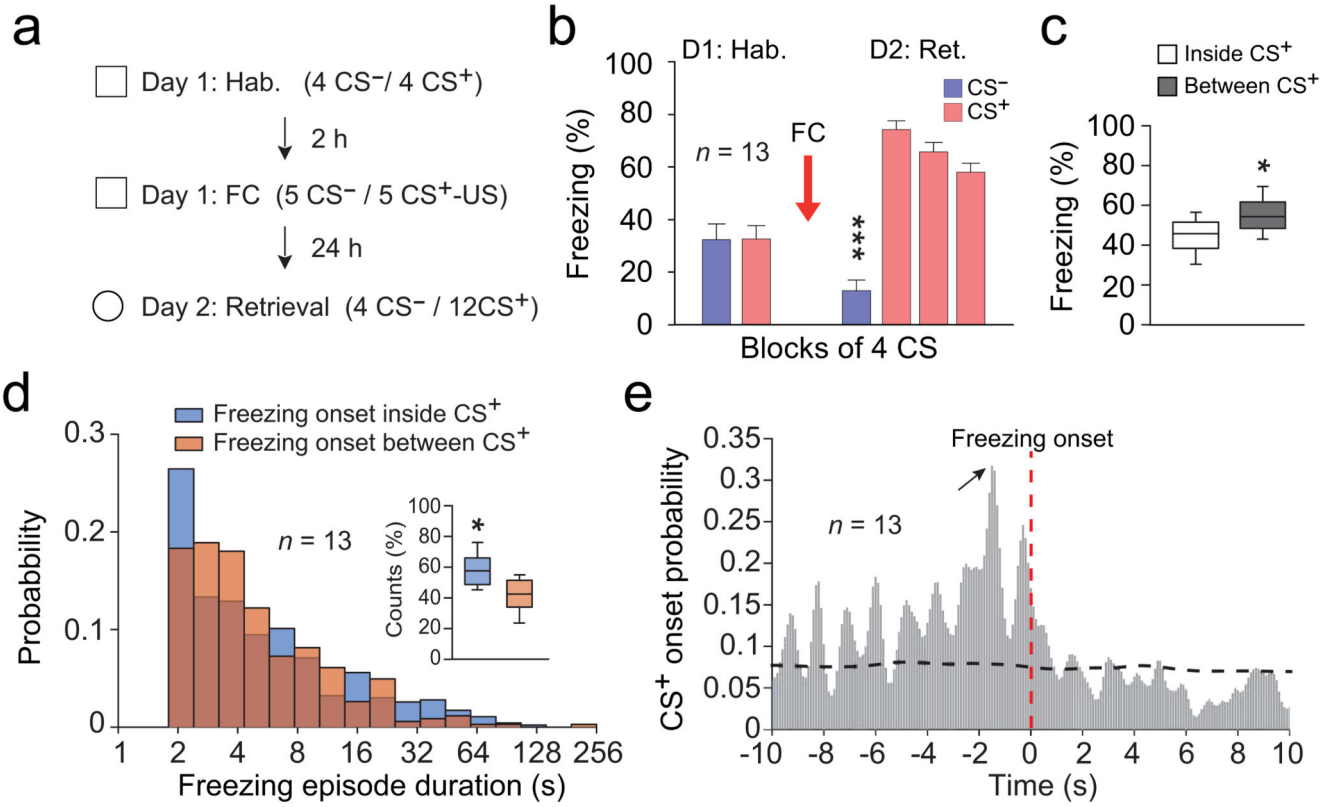

Figure 1. Freezing behaviour is triggered by internally generated mechanisms

(**a**) Experimental protocol. (**b**) Behavioural results. During habituation (Hab.), mice ($n = 13$) exhibited low freezing during CS^- and CS^+. Following conditioning (Day 2: Retrieval), CS^+ (CS^+ 1-12 grouped in blocks of 4) induced high freezing in comparison to CS^- (Paired *t*-tests, CS^- versus each CS^+ block: t(12) = −11.929; t(12) = −11.929; t(12) = −8.442, *** all *Ps* < 0.001). (**c**) Percentage of freezing exhibited during and between CS^+ presentations (Paired *t*-test, freezing inside versus between CS^+: t(12) = −2.480, * $P = 0.029$). (**d**) Distribution probability for freezing episode duration as a function of whether freezing was initiated inside or between CS^+ presentations. Inset: Percentage of freezing episodes initiated inside or between CS^+ presentations ($n = 13$ mice, Paired *t*-test, t(12) = 2.762, * $P = 0.016$). (**e**) Cross-correlation analysis performed between freezing and CS^+ onset ($n = 13$ mice, 100 ms bins). Red vertical dotted line represents freezing onset. Black horizontal dotted line represents significance level. Black arrow indicates the highest probability for CS^+ onset at 1.5 s prior freezing onset. Error bars: mean ± s.e.m. For box plots, the middle, bottom and top lines correspond to the median, lower quartile and upper quartile and whiskers to lower and upper extremes minus lower quartile and upper quartile, respectively..

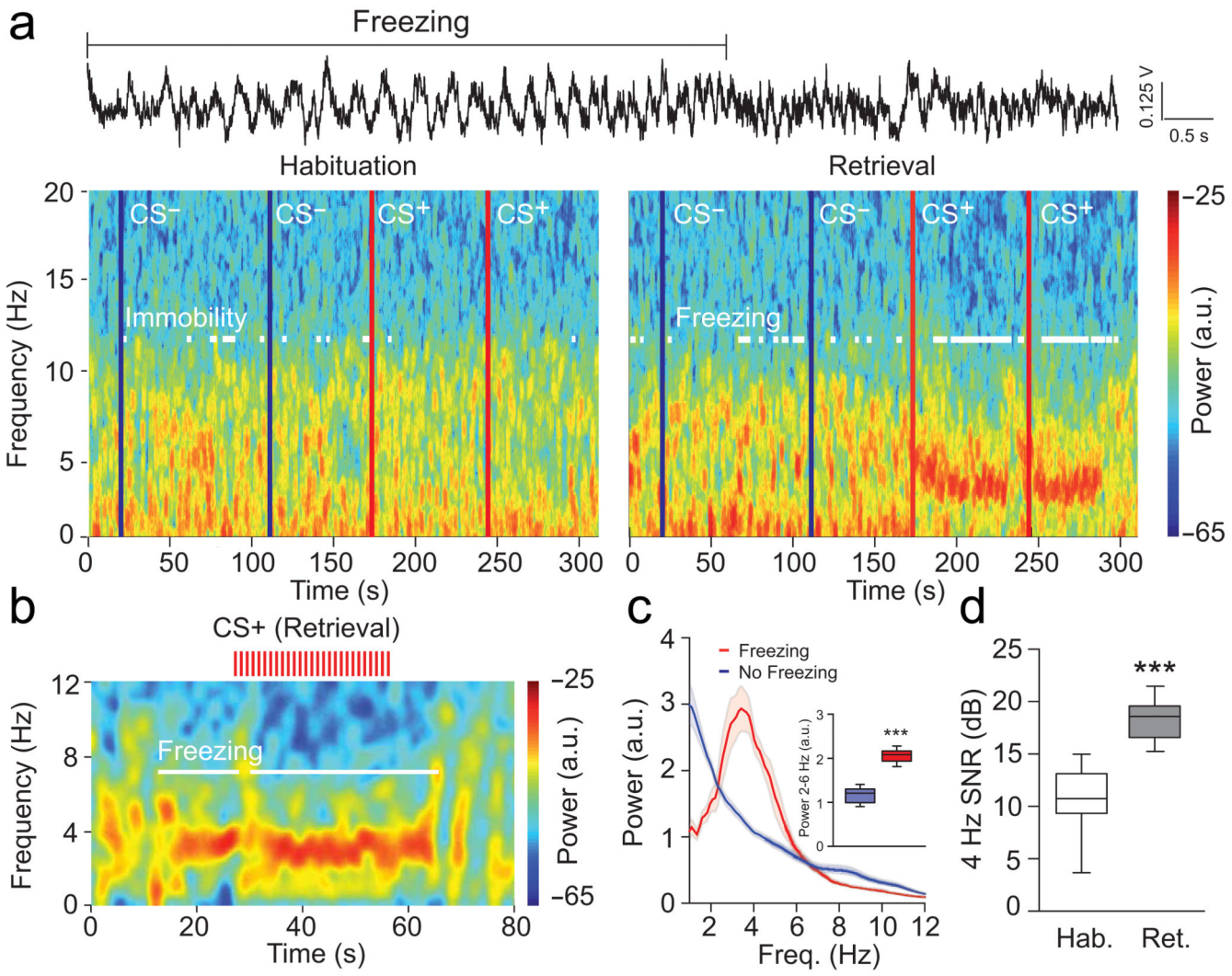

Figure 2. Emergence of dmPFC 4 Hz oscillations during freezing behaviour

(**a) Top**, Representative dmPFC raw LFP traces recorded during Retrieval. 4 Hz oscillatory activity is prominent during freezing behaviour. **Bottom**, Representative spectrograms of dmPFC LFPs during Habituation and Retrieval sessions during CS^{-} and CS^{+} presentations (blue lines: CS^{-} onset; red lines: CS^{+} onset; Hab. and Retrieval: CS^{-} 3 and 4 and CS^{+} 1 and 2). White lines on the spectrogram indicate immobility/freezing episodes. (**b**) Representative spectrogram of dmPFC LFPs at a finer time resolution before, during, and after presentation of a CS^{+} during Retrieval (each red tick represents a single CS^{+} pip). White lines on the spectrogram indicate freezing episodes. (**c**) Averaged power spectrum of dmPFC LFPs recorded during Retrieval for freezing and no freezing periods ($n = 13$ mice, shaded areas: mean ± s.e.m.). Inset: Averaged dmPFC 2-6 Hz power during Retrieval for freezing and no freezing periods (Paired t-test, Freezing versus No Freezing: $t(12) = -14.884$, *** $P < 0.001$). (**d**) Averaged signal to noise ratio (SNR) of 4 Hz oscillation (2-6 Hz) during Habituation and Retrieval ($n = 12$ mice, paired t-tests, Hab. versus Retrieval: dmPFC: $t(11) = -6.805$, *** $P < 0.001$). Shaded areas and error bars: mean ± s.e.m. For box plots, the middle, bottom and top lines correspond to the median, lower quartile and upper quartile and

whiskers to lower and upper extremes minus lower quartile and upper quartile, respectively. For representative examples (**a**, **b**), similar traces were observed for the 13 animals used in these experiments.

Europe PMC Funders Author Manuscripts

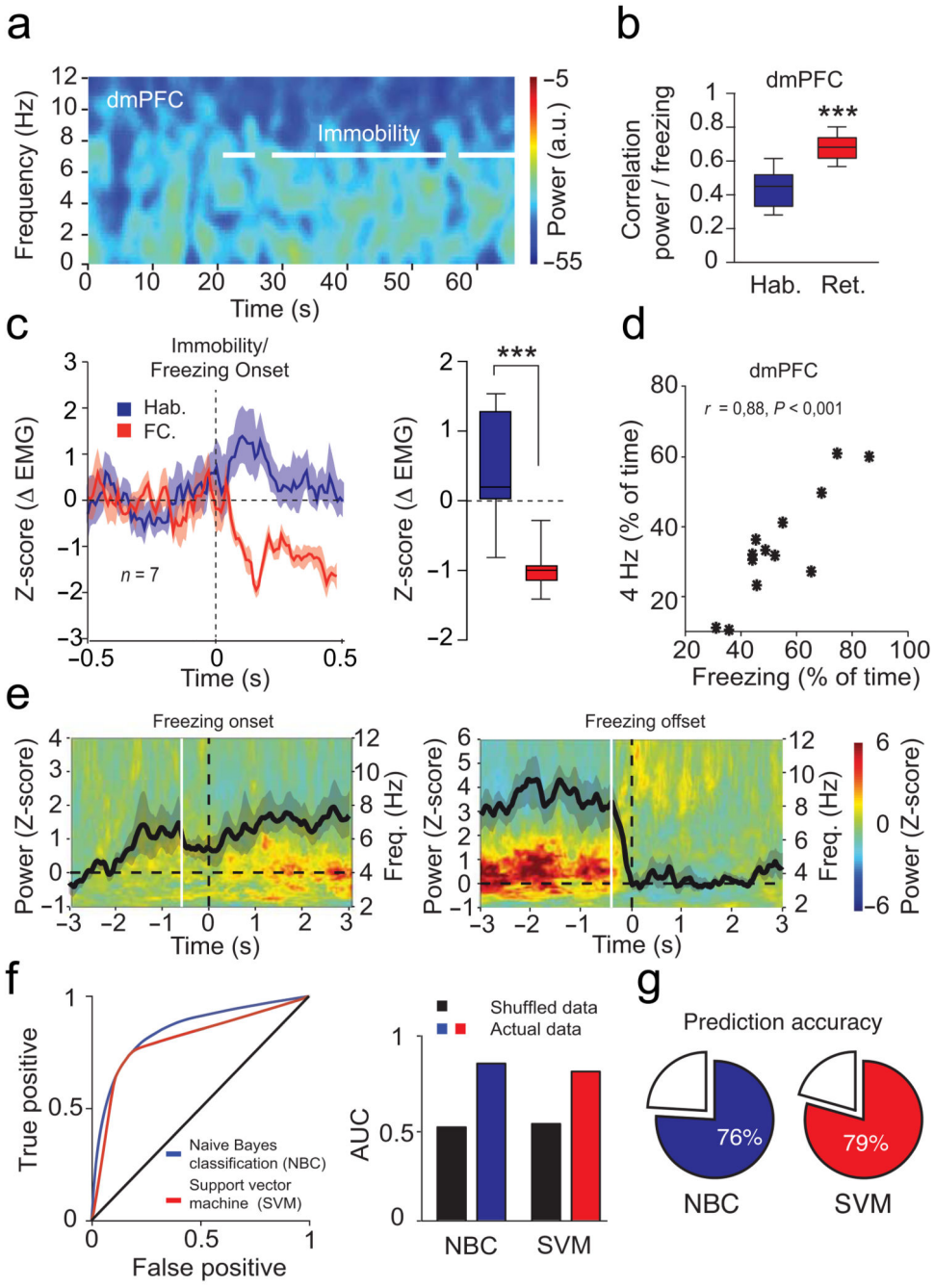

Figure 3. dmPFC 4 Hz predict freezing

(**a**) Spectrograms of dmPFC LFP during Habituation (Hab.). White lines indicate immobility. **(b)** Correlation between dmPFC 4 Hz power and freezing during Hab. and Retrieval ($n = 13$ mice, paired t-tests: t(12) = 6.134, *** $P < 0.001$) (**c**) **Left**, Mean Z-score for neck electromyography (Δ EMG) during immobility/freezing ($n = 7$ mice) for CS^+ presentations. **Right**, Averaged Δ EMG (0-500 ms post-CS^+, Mann-Whitney U test, Hab. versus FC: U = 0, *** $P < 0.001$). (**d**) Correlation between freezing and dmPFC 4 Hz ($n =$ 13 mice; Pearson's $r = 0.88$, $P < 0.001$). (**e**) Averaged freezing onset (**left**) and offset (**right**)

-triggered z-scored spectrograms of dmPFC LFPs (n = 13 mice; black lines: averaged z-scored power envelope; white lines: first significant bin of 4 Hz power changes (increase: −0.53 ± 0.31 sec; decrease: −0.39 ± 0.10 sec; one sample t-test: first significant bin versus hypothetical mean = 0, increase: t(12) = 19.207, $P < 0.001$; decrease: t(12) = 16.615, $P < 0.001$)). **(f) Left**, Receiver operating characteristics (ROC) analysis performed on Naïve Bayes (NBC) and Support Vector Machine (SVM) classifiers trained on dmPFC 4 Hz signal to noise ratio (SNR) during freezing. **Right**, averaged area under the curve for both classifiers versus shuffled data. **(g)** Accuracy of both classifiers to predict freezing. a.u.: arbitrary units. Power in log scale. Shaded areas and error bars: mean ± s.e.m. For box plots, the middle, bottom and top lines correspond to the median, lower and upper quartile and whiskers to lower and upper extremes minus lower quartile and upper quartile, respectively. For the representative example in (**a)**, similar traces were observed for the 13 animals used in these experiments.

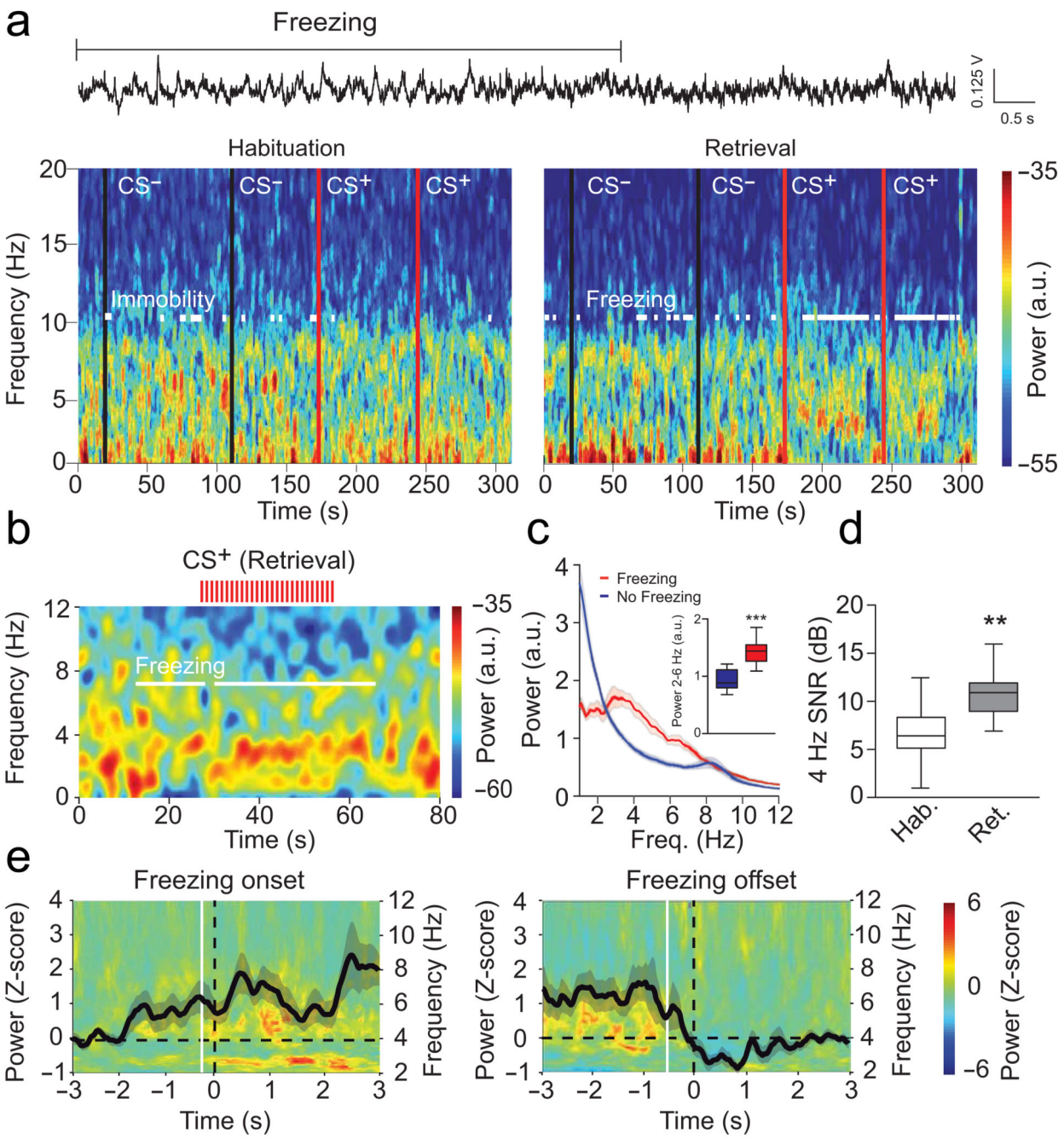

Figure 4. BLA 4 Hz emerge during freezing

(**a) Top**, Representative BLA LFP traces recorded during Retrieval. **Bottom**, Spectrograms of BLA LFPs during Hab. and Retrieval during CS^- and CS^+ (black lines: CS^- onset; red lines: CS^+ onset). White lines indicate immobility/freezing. (**b**) Spectrogram of BLA LFPs before, during, and after presentation of a CS^+ during Retrieval (red ticks represent single CS^+ pip). White lines indicate freezing. (**c**) Averaged power spectrum of BLA LFPs recorded during Retrieval for freezing and no freezing ($n = 13$ mice). Inset: Averaged BLA 2-6 Hz power during Retrieval for freezing and no freezing (Paired *t*-test, Freezing versus

Europe PMC Funders Author Manuscripts

No Freezing: t(12) = 6.077, *** $P < 0.001$). (**d**) Averaged 4 Hz signal to noise ratio (SNR) during Habituation and Retrieval ($n = 12$ mice, paired t-tests, Hab. versus Retrieval: BLA: t(11) = 3.334, ** $P = 0.003$). (**e**) Averaged freezing onset (**left**) and offset (**right**) -triggered z-scored spectrograms of BLA LFPs ($n = 13$ mice, black lines: averaged z-scored power envelope; white lines: first significant bin of 4 Hz power changes (increase: −0.27 ± 0.20 sec; decrease: −0.46 ± 0.22 sec; one sample t-test: first significant bin versus hypothetical mean = 0, increase: t(12) = 10.976, $P < 0.001$; decrease: t(12) = 34.372, $P < 0.001$)). a.u.: arbitrary units. Spectral power in log scale. Shaded areas and error bars: mean ± s.e.m. For box plots, the middle, bottom and top lines correspond to the median, lower and upper quartile and whiskers to lower and upper extremes minus lower quartile and upper quartile, respectively. For representative examples (**a**, **b**), similar traces were observed for the 13 animals used in these experiments.

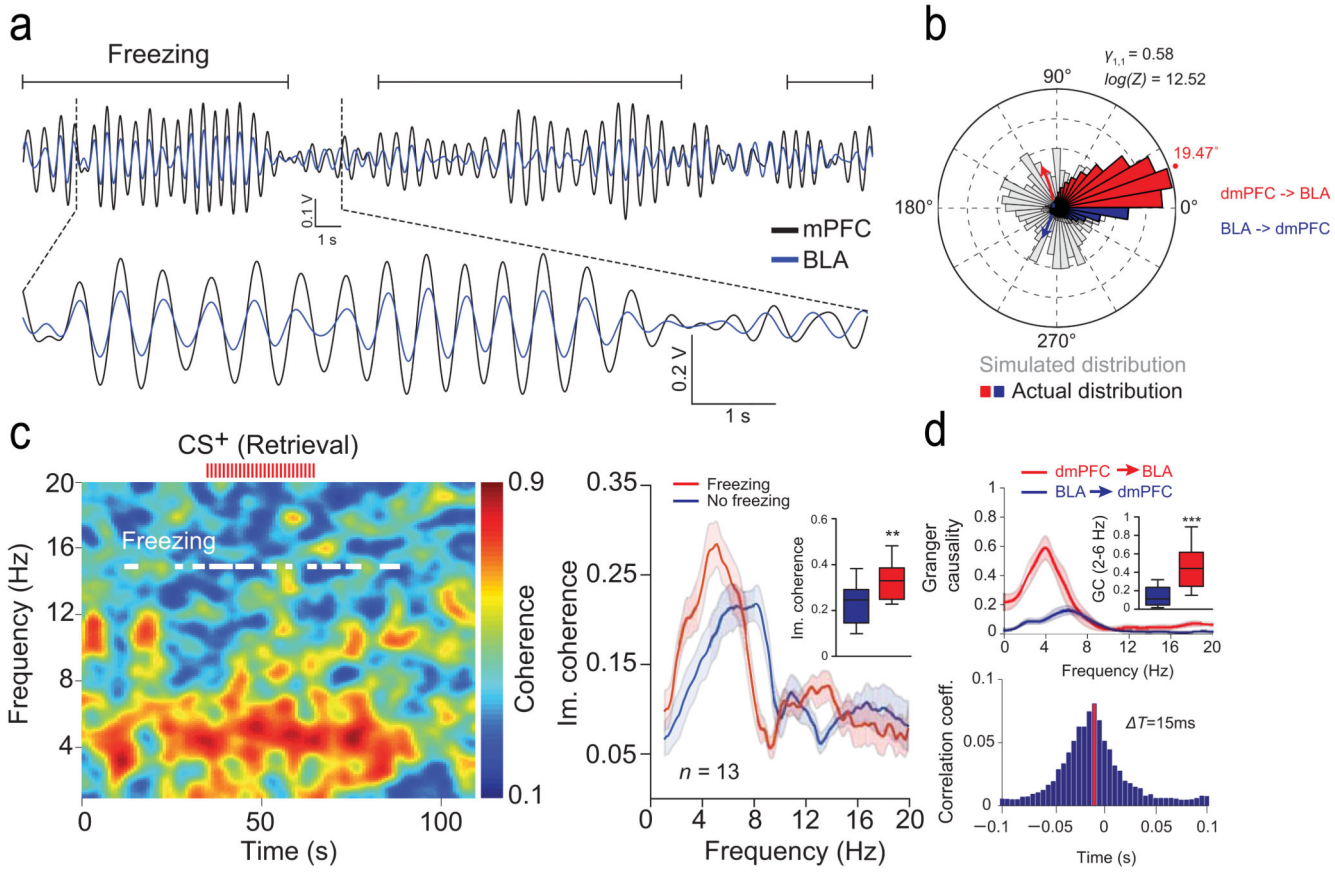

Figure 5. Synchronization of dmPFC and BLA 4 Hz during freezing

(**a**) Overlaid filtered (2-6 Hz) dmPFC and BLA LFP traces illustrating synchronized 4 Hz during freezing. (**b**) Circular distribution of the phase differences between dmPFC and BLA LFPs recorded for freezing during Retrieval compared to a control bootstrap simulated phase distribution (n = 13 mice). (**c**) **Left**, Representative coherogram for dmPFC and BLA LFPs recorded during Retrieval during CS^+ (red ticks represent individual CS^+ pip). White lines indicate freezing. **Right**, Averaged dmPFC and BLA LFPs imaginary coherence (Im. coherence,) for Freezing and No freezing during Retrieval (n = 13 mice). Inset: Averaged peak of Im. coherence for Freezing and No freezing during Retrieval (Paired t-test, Freezing versus No Freezing: t(12) = 3.933, * P = 0.002). (**d**) **Top,** Granger Causality (GC) analysis performed between dmPFC and BLA LFPs during freezing (n = 13 mice). Inset: Averaged Granger Causality (2-6 Hz) performed between dmPFC and BLA LFPs during freezing (Retrieval, Paired t-test, dmPFC → BLA versus BLA → dmPFC: t(12) = −5.940, *** P < 0.001). **Bottom,** Averaged cross-correlogram performed between dmPFC and BLA LFPs (2-6 Hz). The peak (red bar) and negative skewness of the distribution indicate that dmPFC 4 Hz oscillations lead the BLA oscillatory activity by 15 ms (n = 13 mice). Shaded area and error bars: mean ± s.e.m. For box plots, the middle, bottom and top lines correspond to the median, lower and upper quartile and whiskers to lower and upper extremes minus lower quartile and upper quartile, respectively. For representative examples (**a**, **c**), similar traces were observed for the 13 animals used in these experiments.

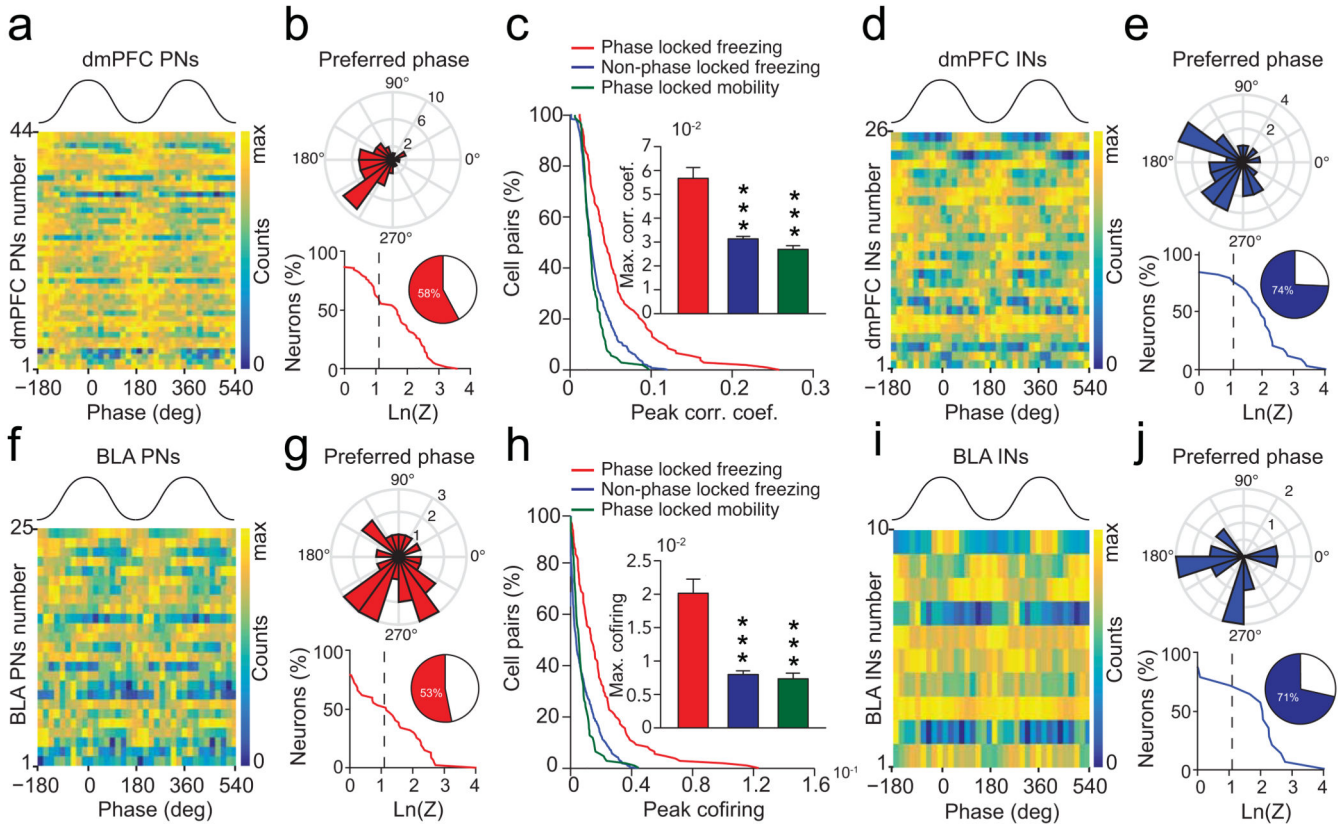

Figure 6. 4 Hz oscillations synchronize dmPFC-BLA spiking activity

(**a, d, f, i**) Phase distribution relative to 4 Hz oscillations for dmPFC (**a, d**) and BLA (**f, i**) putative excitatory neurons (PN) (**a, f**) or putative inhibitory interneurons (IN) (**d, i**). (**b, g, e, j**) Circular distribution of the 4 Hz preferred phase for populations of dmPFC (**b, e, top**) and BLA (**g, j, top**) phase-locked PNs (**b, g**) and INs (**e, j**) during freezing (dmPFC: 44 PNs and 26 INs; BLA: 25 PNS and 10 INs) and cumulative distribution of log-transformed Rayleigh's test Z of dmPFC (**b, e, bottom**) and BLA (**g, j, bottom**) PNs (**b, g**) and INs (**e, j**). Inset, percentage of dmPFC and BLA neurons significantly phase-locked to 4 Hz oscillations. Dashed line, significant 4 Hz phase locking threshold (ln(Z)= 1.097, * $P < 0.05$, dmPFC: 44/92 PNs and 26/35 INs; BLA: 25/72 PNs and 10/15 PNs). (**c, h**) Cumulative distribution of peak correlation coefficient (**c**) and co-firing index (**h**) for pairs of dmPFC and BLA phase-locked and not phase-locked neurons during freezing and mobility. Insets: Maximum correlation coefficient (**c**) and co-firing index (**h**) for all pairs of recorded dmPFC and BLA neurons (Phase-locked pairs: $n = 180$; Non Phase-locked pairs: $n = 911$, Mann-Whitney U test, top and bottom, phase-locked pairs during freezing versus mobility or non phase-locked pairs: U = 50313, 7893, 16200, 9413, ** $P < 0.001$, *** $P < 0.001$). Error bars: mean ± s.e.m.

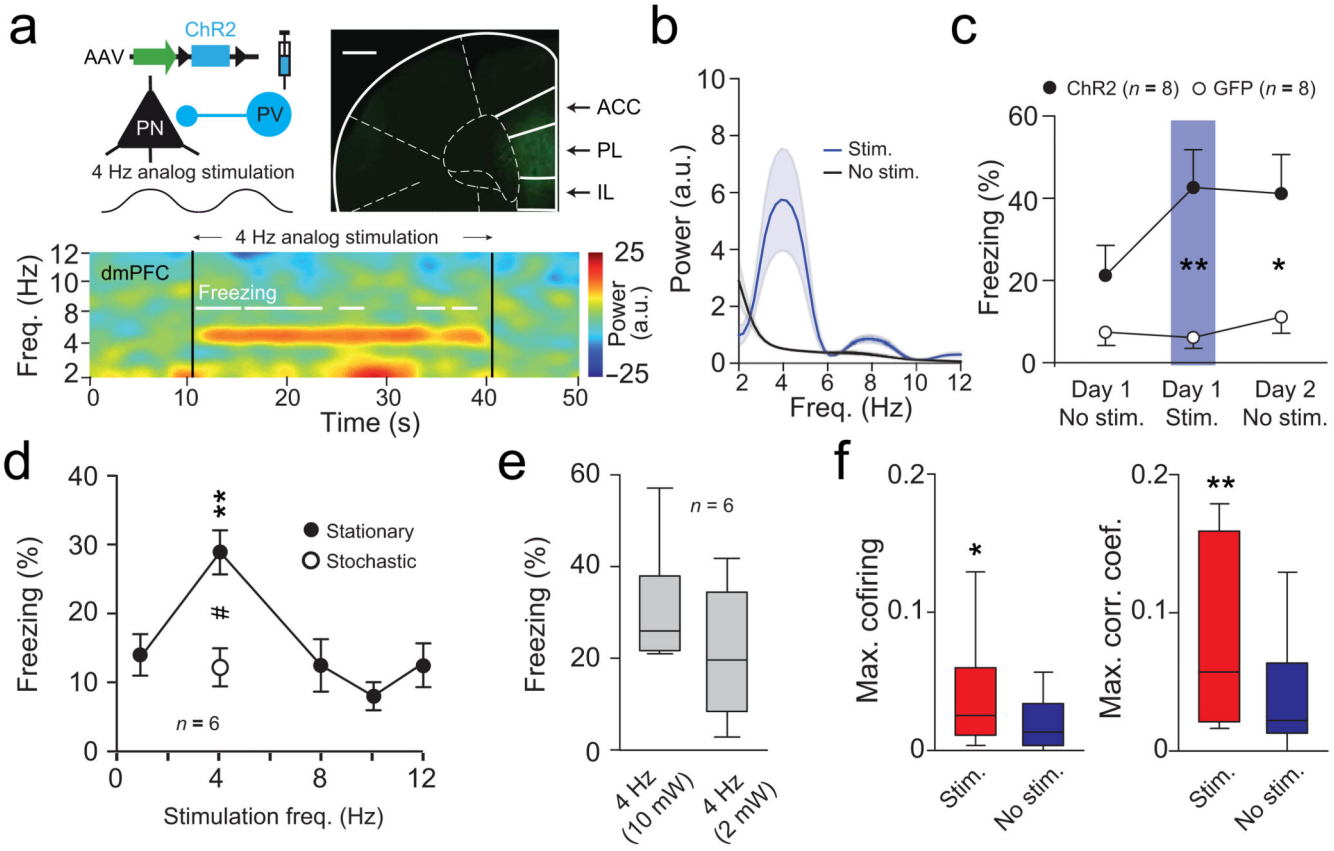

Figure 7. Optogenetic induction of dmPFC 4 Hz drives freezing

(**a**) **Top left**, Strategy used to activate PV INs. **Top right**, dmPFC micrograph from a PV-IRES-Cre mouse expressing ChR2. Scale bar = 0.5 mm. **Bottom,** Spectrogram during 4 Hz analog stimulation. (**b**) Averaged normalized LFP power spectra of dmPFC LFPs during (Stim.) and outside (No stim.) stimulation ($n = 8$). (**c**) Percentage of freezing for ChR2 ($n = 8$) or GFP ($n = 8$) mice before, during and after 4 Hz induction (two way ANOVA repeated measures; group: $F_{(1,14)} = 0.868$, $P = 0.367$, time $F_{(1,2)} = 8.926$, $P = 0.001$, group × time $F_{(1,28)} = 6.925$, $P = 0.0036$); Unpaired *t*-tests: Day 1: Stim. t(14) = 3.712, ** $P = 0.002$; Day 2: No stim., t(14) = 2.758, * $P = 0.013$). (**d**) Percentage of freezing for ChR2 mice ($n = 6$) during analog stimulation at 1, 4, 8, 10, 12 Hz (Stationary) or using a 4 Hz stochastic waveform (Stationary: One way repeated measures ANOVA: $F_{(5,4)} = 8.618$, *** $P < 0.001$; Bonferroni corrected Paired *t*-tests: 4 versus 1 Hz: t(5) = 5.927, ** $P = 0.0019$; 4 versus 8 Hz: t(5) = 4.712, ** $P = 0.0053$; 4 versus 10 Hz: t(5) = 7.632, *** $P < 0.001$; 4 versus 12 Hz: t(5) = 4.009, ** $P = 0.01$; Paired *t*-test: 4 Hz stationary versus stochastic: t(5) = 3.533, # $P < 0.016$). (**e**) Percentage of freezing for ChR2 ($n = 6$) mice during dmPFC 4 Hz analog stimulation at 2 or 10 mW (Paired *t*-test: t(5) = 0.951, $P = 0.385$). (**f**) Maximum correlation and co-firing index for pairs of dmPFC and BLA neurons during and outside stimulation ($n = 31$ pairs, Mann-Whitney, U = 326 and 278, *$P = 0.03$; **$P = 0.004$). a.u.: arbitrary units. Power in log scale. Shaded area and error bars: mean ± s.e.m. For box plots, the middle, bottom and top lines correspond to the median, lower and upper quartile and whiskers to lower and upper extremes minus lower quartile and upper quartile, respectively. For

Europe PMC Funders Author Manuscripts

representative examples (**a**), similar images and traces were observed for the 16 (**top,** 8 ChR2 and 8 GFP mice) and 8 (**bottom,** 8 ChR2 mice) animals used in these experiments.

Europe PMC Funders Author Manuscripts